Radiation Physics and Chemistry 229 (2025) 112413

Contents lists available at ScienceDirect

Radiation Physics and Chemistry

journal homepage: www.elsevier.com/locate/radphyschem

Calculation of dose conversion coefficients for radiation workers in various postures

Min Chae Kim [a], Hyoungtaek Kim [a,*], Heagin Han [b], Yoomi Choi [a], Sora Kim [a], Jungil Lee [a], Byung Il Min [a], Kyungsuk Suh [a], Chan Hyeong Kim [c]

[a] Korea Atomic Energy Research Institute, 989-111 Daedeok-daero, Yuseong-gu, Daejeon, 34057, Republic of Korea
[b] National Cancer Institute, National Institute of Health, Bethesda, MD, 20852, USA
[c] Department of Nuclear Engineering, Hanyang University, 222, Wangsimni-ro, Seongdong-gu, Seoul, 04763, Republic of Korea

A R T I C L E   I N F O

Handling editor: Chris Chantler

Keywords:
Mesh-type phantom
Monte Carlo simulation
Working postures
Personal dosimeter
Dose conversion coefficients

A B S T R A C T

The present study investigates the impact of various body postures on dose assessment. Existing radiation protection systems that assume a standing posture are generally valid in most situations; however, they may not be effective in assessing the dose received by individuals in specific conditions such as radiation accidents. To address this, we used the Geant4 simulation code and mesh-type reference computational phantoms (MRCPs) to model and calculate the dose conversion coefficients (DCCs) for 19 representative working postures. These representative postures were developed by referencing existing industrial posture categories, combining movements of arms, torso, and legs. The exposure geometries considered in the present study include generalized parallel beams such as anterior-posterior (AP), posterior-anterior (PA), left-lateral (LLAT), and right-lateral (RLAT), and isotropic exposures from all sides (rotational (ROT) and isotropic (ISO)), along with semi-isotropic forms of ground and ceiling contamination ranging from 30 cm to 50 m in radius. The results demonstrate that the dose ratios between a personal dosimeter and whole-body (i.e. DCCs) are significantly influenced by the body posture and the exposure geometry. Particularly, exposures involving significant body shielding, such as ground and ceiling contamination and PA direction exposures, were mainly affected by the degree of torso bending. For instance, a DCC of 2.3 was recorded for a posture with approximately 45 degrees of torso bending under PA exposure. Additionally, in a ground contamination scenario having a 1 m radius beam, DCCs ranged from 0.8 to 2.5 depending on the degree of torso bending, and in a 2 m radius ceiling contamination scenario, DCCs of 1.2–1.7 were observed in postures with 90 degrees of torso bending. These findings emphasize the importance of posture-specific dose assessments in various contamination scenarios.

1. Introduction

Standardized and simplified external exposure geometries for an individual in a standing posture are addressed in the International Commission on Radiological Protection (ICRP) publication (ICRP, 2010) in response to the ICRP general recommendations for radiation workers (ICRP, 2007). On the other hand, a dose assessment that takes into account the posture of the exposed person may be of more interest in radiological accidents. Notably, in an exposure incident from mammography equipment in Dakar and Abidjan in 2006, the kneeling posture of the victim was considered in the dose reconstruction (Clairand et al., 2008). Similarly, specific working postures were evaluated for the tragic accident at the nuclear fuel processing facility in Tokai-Mura in 1999 (Endo and Yamaguchi, 2003).

In such scenarios, a numerical calculation using posture-modified anthropomorphic computational models can provide reasonable estimates. Due to this perspective, a research team at Rensselaer Polytechnic Institute has developed a computational human for animated dosimetry (CHAD) phantom utilizing motion capture information (Vazquez et al., 2014). Besides, the human model used in the radiological environment modeling system developed by Sandia National Laboratory can represent various postures using 50 customizable joints (Breazeal et al., 1996). The Oak Ridge National Laboratory has developed a computational phantom model called PIMAL (Phantom with Movable Arms and Legs), which allows for enhanced simulation flexibility by enabling joint rotation in areas such as the shoulders, elbows,

* Corresponding author.
E-mail address: kht84@kaeri.re.kr (H. Kim).

https://doi.org/10.1016/j.radphyschem.2024.112413
Received 14 June 2024; Received in revised form 30 September 2024; Accepted 18 November 2024
Available online 22 November 2024

hips, and knees (Akkurt and Eckerman, 2007; Dewji et al., 2017). These posture-modified computational phantoms/models can be applied to scenarios where exposure information is well-recorded such as in a workplace monitored by closed-circuit television (CCTV). However, if the information is uncertain, e.g. a situation where only a rough sketch of the posture is available from interviews, a dose assessment can be made by selecting one of the most possible representatives. In this context, the five postures, such as standing, bending, kneeling, squatting, and walking, were proposed using a recently developed mesh-type human phantoms (Yeom et al., 2019). While these five postures are worth discussing as representative of radiation workers, there is a necessity for a systematic approach to classification considering ergonomics and personal dosimetric points of view.

Meanwhile, in routine dosimetry, Hp(10) has been used as a surrogate for assessing effective dose conservatively, which pertains to stochastic radiological effects. On the other hand, in the event of a radiation accident, organ/tissue-averaged absorbed doses are estimated and used to consider deterministic effects. It is important to note that, at the current stage of accident dosimetry, there is a lack of consensus on the definition of a whole-body dose which can provide an overall deterministic risk for a victim (Eakins and Ainsbury, 2018). In the field of dose conversion in accident scenarios, one study calculated the whole-body absorbed dose (D_{WB}) of a voxel computational phantom (calculated as the average of organ doses according to mass ratio) (Eakins and Kouroukla, 2015), while another study used an effective dose by summing the organ doses of a mesh type computational phantom, weighted by the ICRP 103 radiation and tissue weighting factors (Kim et al., 2019). The other study published in 2018 explored several newly defined multi-organ absorbed doses considering the effects of Acute Radiation Syndrome (ARS), proposing D_{GRB} (absorbed dose to the stomach, small intestine, red bone marrow, and brain) and D_{max} (maximum organ dose) as optimum quantities for risk assessment (Eakins and Ainsbury, 2018).

These endeavors have been undertaken to correlate a measured absorbed dose of a fortuitous dosimeter to a risk indicator of the whole-body, based on the assumption that the two values diverge at certain exposure geometry. This situation can also be applicable even for the case where the victim wore a personal dosimeter. For instance, when working with a squatting posture for long periods in a workplace with contamination on the ceiling or floor (Hayashi et al., 2024; Hirouchi et al., 2021), or in an environment where a source is behind the victim, the Hp(10) may no longer estimate effective dose conservatively, potentially underestimating radiological risk. Therefore, several computational studies have taken into account exposures to ground contamination. In the study using the PIMAL phantom, the differences between the upright and torso bending phantoms were compared within plane sources directed upward from below the feet and downward from above the head (Bales and Dewji, 2019; Veinot et al., 2016). Another study modeled an exposure from a floor using a semi-isotropic disc source having a 2 m radius and then provided universal DCCs for infinite floor contamination through fluence normalization (Eakins and Kouroukla, 2015). The ICRP Report 144 published dose coefficients for infinite ground contamination caused by radionuclide fallout or naturally occurring terrestrial sources (ICRP, 2020a). The infinite exposure structure allows calculating universal dose coefficients in a uniform radiation field from the feet to the head. On the other hand, realistic working environments involve sources with limited sizes, such as an operation in a steam generator (Kim and Kong, 2010) and an emergency operation on contaminated water (Hirouchi et al., 2021; Imanaka et al., 2015), where the high dose gradient along the source plane to the individual organs can amplify the discrepancy between Hp(10) and the effective dose or D_{WB}.

In the present study, nineteen representative working postures were developed using mesh-type reference computational phantoms (ICRP, 2020b). Furthermore, this study calculated DCCs of posture-modified phantoms under generalized beams that provide estimates of D_{WB} from a personal dosimeter. Additionally, we discussed the impact of body postures in exposure geometries associated with limited sizes of floor and ceiling contamination.

2. Materials and methods

Simulations were conducted using the Geant4 code (ver. 10.7.3), incorporating the adult male mesh-type reference computational phantom (MRCP) in ICRP-145 (ICRP, 2020b). The height and weight of the phantom were 176 cm and 73 kg. The G4PSEnergyDeposit class was employed to calculate organ/tissue-averaged absorbed doses. For each calculation, a total of 10^9 primary photons were simulated.

The posture of the MRCP was deformed by using Mesh-type Phantom Posture Deformer (MPPD) program developed by Han et al. (2023). For this, 23 joints of the phantom, including the shoulder, elbow, wrist, hip, knee, and ankle, were manually rotated to achieve the desired posture. Note that the MPPD program applies a bounded biharmonic weights algorithm for vertex weight calculations and a dual quaternion skinning algorithm for posture deformation with minimal distortion and protrusion of internal organs. The detailed methodology has been previously reported in the literature.

To systematically develop working postures, we considered the Ovako Working Posture Analysis System (OWAS) (Karhu et al., 1977), the Ergonomic Assessment Worksheet (EAW) (Schaub et al., 2012), and the Rapid Upper Limb Assessment (RULA) (Dockrell et al., 2012). These posture classifications have been proposed for assessing the risk and efficiency of workers in the industry, categorizing major body parts such as the back, arms, and legs into combinable components. For instance, the shape of the back can be straightened, bent, or twisted, while the arms can be below or above shoulder level. Leg positions include straight, sitting, or kneeling. According to these methodologies, Fig. 1 (a) illustrates the body frame as the simplified joint connections of the individual parts. Fig. 1 (b) shows the 3D posture structures that combine the joint information and the posture deformable phantom (i.e. adult male MRCP) provided by Hanyang University. Furthermore, the postures were selected considering the shielding effect of a body part on a personal dosimeter located on the left chest under simplified exposure geometries such as AP, PA, LLAT, and RLAT. Specifically, the back angles of ~0, ~45, and ~90° were chosen considering the different attenuations by the torso to the dosimeter in a PA exposure. In addition, hand positions such as down, in front, and up hand were set so that the dosimeter was unshielded or fully shielded in LLAT and RLAT exposures. The leg shapes are divided into standing, kneeling, and squatting, in correspond to floor exposures that will be discussed later. To minimize the redundancy of the postures, only the left leg was bent in the kneeling postures, considering the shielding effect on the dosimeter located at the left chest in bottom-up irradiation. If the dosimeter was attached to the right chest, or if the right leg was bent while having the dosimeter on the left chest, it was assumed that the expected values from these configurations would be substituted for the results of the standing postures. Each posture is numbered sequentially in the figure and these numbers will be used in the following data and analysis. Regarding the hand positions, the down-hand shapes are confirmed to exhibit similar shielding effects to the up-hand shapes, and some of them are not realistically maintainable. Therefore, the postures shaded in grey were excluded from the calculations and discussions, with posture M111 remaining as a representative.

The dosimeter was constructed as a cylinder shape with a radius of 2.5 cm and a height of 1.1 cm, employing G4_tissue_SOFT_ICRP (density of 1.03 g/cm^3). To approximate the deep dose equivalent, i.e. Hp(10), energy deposition was calculated in a smaller cylinder located inside, 1 cm away from the dosimeter's surface, which had dimensions of 1.5 cm in radius and 0.1 cm in height. The detector was positioned parallel to the surface plane of the left chest and placed approximately 1 cm away from the chest. The absorbed dose of the detector (D_{Det}) exhibits a relatively high statistical uncertainty (1–23%) due to its small size, and a

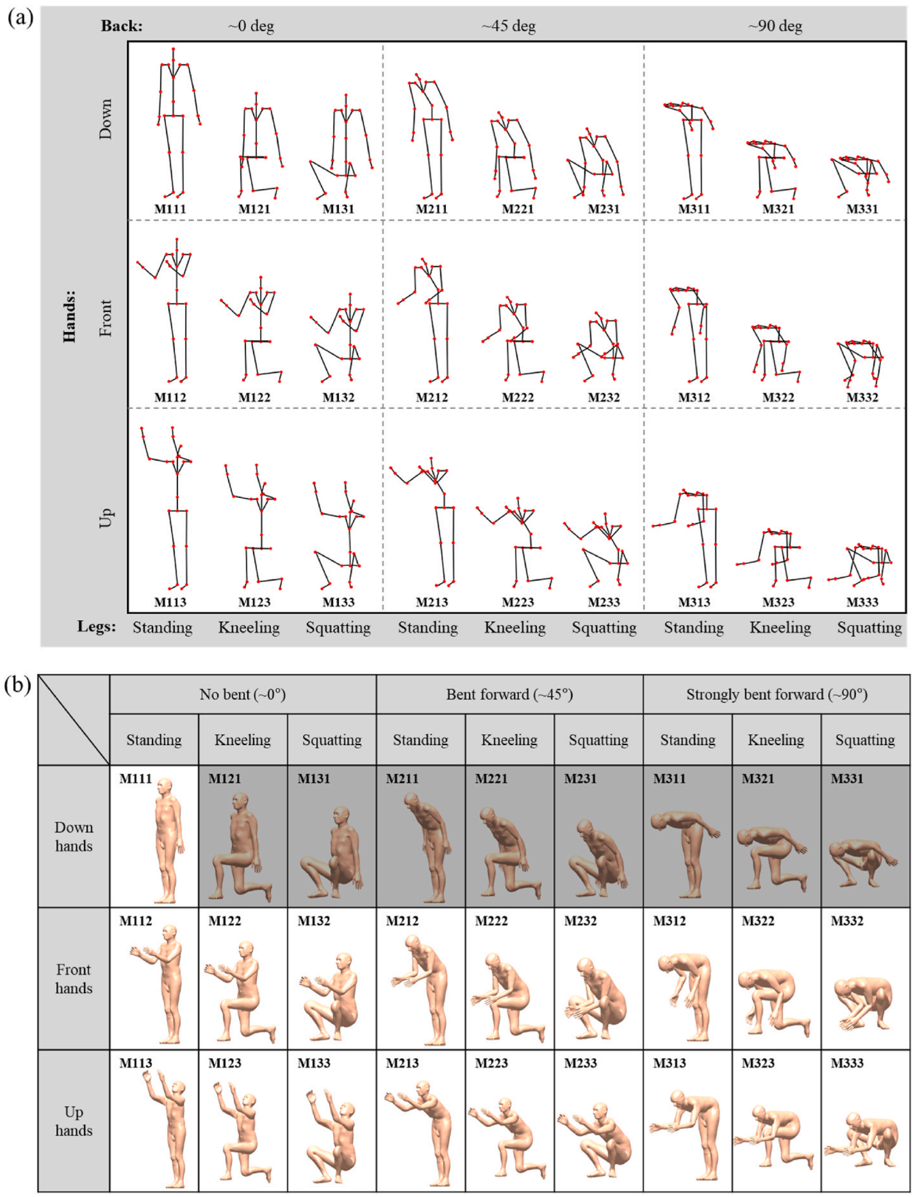

Fig. 1. Representative working postures (a) constructed using the joints of body parts and (b) constructed using the posture-deformable phantom. The postures are classified according to the degree of back bending, leg shape, and hand position and are labeled accordingly. The grey-colored postures are displayed by the logic of the classification but are not considered in this study.

corresponding error bar ($k = 2$) will be given.

There are several candidates for the risk indicator of the whole-body, such as effective dose, D_{WB}, D_{GRB}, and D_{max} (Eakins and Ainsbury, 2018). In the present study, D_{WB} was used and the DCC was calculated by dividing D_{WB} by D_{Det}. In the whole calculation, the statistical uncertainty of D_{WB} was less than 0.1%.

Three radioisotopes, Ir-192, Cs-137, and Co-60, were used for exposure. Exposure directions employed generalized parallel beams such as AP, PA, LLAT, and RLAT using a plane disc source with a 1.5 m radius. The ROT exposure was calculated as the average of the previous four orthogonal exposures. To define the ISO beam, a spherical shell with a 2 m radius that emits photons inwards semi-isotropically was designed. This type of beam shape has been addressed in previous research for DCC calculation (Eakins and Kouroukla, 2015). In the ISO exposure, the center of the phantom box was located at the center of the sphere. The phantom box, containing the MRCP, changes size and center when different postures are selected.

Additionally, the floor contamination was indicated as the bottom-to-top (BT) direction, with a parallel beam (BT_{para}) having a 2 m radius or a semi-isotropic beam (BT_{iso}) ranging from 30 cm to 50 m radius. In this case, the source was designed as a flat disc shape, centered on the x-y center of the phantom box, and placed 1 cm below the toes, as shown in Fig. 2 (a). Although the BT_{para} beam is unrealistic, it was used to investigate the pure geometric influence of postures related to ground contamination, such as squatting and kneeling.

To achieve a low statistical error, extensive computational time was expected for the semi-isotropic beams having more than a 2 m radius. Therefore, beam biasing with a segmented source structure was applied. For example, the BT_{iso} beam with more than 2 m radius combines the 2 m circular source and several annular-shaped sources (i.e. annular of inner/outer diameters: 2/5 m, 5/10 m, 10/20 m, 20/50 m), each having maximum latitude beam biasing angles of 45, 68.2, 78.7, and 84.3°. To ensure that each source shape has the same fluence at the surface, the summation was made by dose per fluence using the area of each source structure. The ceiling contamination was indicated as the top-to-bottom (TB) direction, designed analogously to the BT exposures, such as a

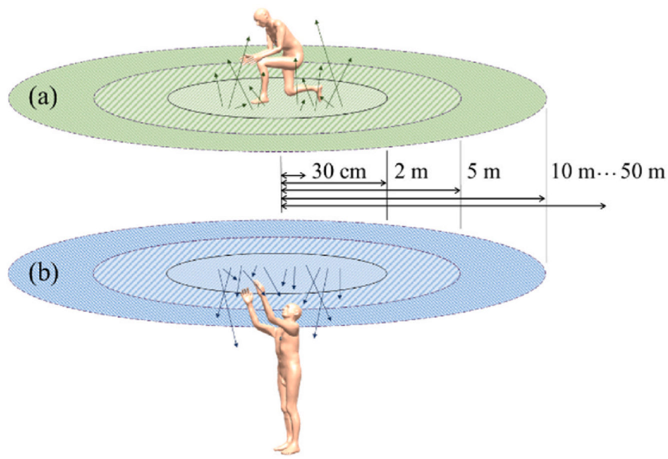

Fig. 2. Schematic of (a) BT_{iso} and (b) TB_{iso} beams. For beams larger than a 2 m radius, it was calculated as the sum of a 2 m circular beam and annular beams.

parallel beam (TB_{para}) having a 2 m radius or a semi-isotropic beam (TB_{iso}) ranging from 30 cm to 50 m radius, located 2.5 m above the floor as shown in Fig. 2 (b).

3. Results and discussions

3.1. Fluence calculation

The absorbed dose in materials is calculated by dividing the accumulated energy by the mass and the number of primary particles, representing the dose introduced by a single emitted particle in a given source structure. To eliminate the dependence on the source structure, a dose per fluence can be obtained by dividing by the reciprocal of the source area, allowing for valid comparison between doses. In this case, all materials being compared are considered to be located in the same fluence, as in a parallel beam. However, in the proposed ISO, BT_{iso}, and TB_{iso} scenarios, fluence depends on location. This indicates that the shielding effect of the human body is not the only factor causing differences between D_{Det} and D_{WB}. Therefore, fluences according to the location in isotropic emitting sources should be considered.

In the ISO field, fluence was calculated using the F4 tally of the MCNP6.2 code (Werner et al., 2018). Fluence detectors, each with a 1 cm radius, were positioned within a 2 m radius ISO beam sphere at distances ranging from 5 to 50 cm from the sphere's center, representing typical organ locations. The surrounding materials, including the inside of the detector, were all filled with air, and 662 keV monoenergetic photons were applied. The statistical uncertainty for all fluence detectors was below 1%. The fluence variation among the detectors was less than 1.5% depending on their positions, with an average fluence of approx. 2.0E-6/cm^2 being used.

For the BT_{iso} field, the fluence ratio according to the distance from the center surface of the disk was calculated using two methods, as depicted in Fig. 3. First, a Monte Carlo calculation, similar to the ISO case, was performed by placing the fluence detectors (1 cm radius) from 2 to 170 cm from the beam surface. Second, the result was mathematically cross-checked by integrating the fluences from a small area of a thin annular source as expressed as follows:

$$Fluence \cong \int_0^R \frac{F_0 2\pi r}{r^2 + d^2} dr \tag{1}$$

where R is the radius of the disc source, r is the radius of the sub-annular shape source with a micro thickness of dr, d is the distance from the center of the annular source to the detector position where fluence is calculated, and F_0 is the unit fluence from a micro area ($da = dr \times rd\theta$) of the annular source at the reference point (i.e. $r^2+d^2 = 1$).

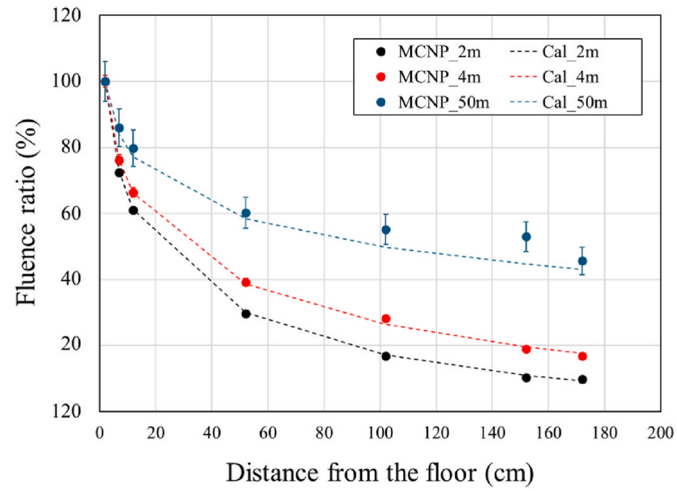

Fig. 3. Fluence ratio as a function of height for the BT_{iso} beam calculated using MCNP6.2 and Eq. (1). The data are normalized to the fluence at the 2 cm position.

In the case of an infinite size source using Eq. (1), a uniform fluence was achieved, but at the 50 m radius, the largest size source in this study, height dependency was observed. As the radius R of the source increased, the decrease in fluence ratio became smaller. Considering the reference standing posture (M111), the decrease rate between the two heights where major organs are located, i.e. 100 and 150 cm, was 36%, 26%, and 10% for the radius of 2, 4, and 50 m, respectively. In contrast, for the kneeling and squatting postures, the decrease rate between 50 and 100 cm, where major organs are located, was 43%, 32%, and 15%, respectively.

The fluence of the TB_{iso} field can be estimated from Fig. 3 by assuming the 250 cm height as the ground and the 75 cm height as the head position. This assumption allows us to know that the major organs are relatively evenly exposed to fluence. Due to the fluence dependency, only DCCs were provided for the BT_{iso} and TB_{iso} fields in Sections 3.3 and 3.4.

3.2. DCCs for generalized beams

Fig. 4 shows the dose per fluence and DCCs for the postures in Fig. 1 under exposures to the generalized beam of Co-60. The same data sets for Cs-137 and Ir-192 isotopes are presented in Figures A1 and A2 of Supplementary Materials, respectively. The first point of interest is whether the postures and detector placements exhibit reasonable results within the generalized beams. This includes assessing whether the body shielding effects from different posture variations are in the expected range and whether the logic of the posture variation which was described in the method section will show systematic changes. Additionally, the effect of the differences in dosimeter placement can be investigated. The second, more significant point of interest involves confirming cases where the D_{Det} fails to conservatively estimate D_{WB}, i.e. when the DCC exceeds 1. The third focus is situations where D_{Det} significantly overestimates D_{WB}, i.g. when the DCC is lower than 0.5, an arbitrary value for the present analysis.

In Fig. 4 (a), the D_{WB} of all modified postures shows reduced values of up to 31% compared to the reference posture (M111). The decrease rate is mainly proportional to the degree of the torso bending, suggesting it stems from the upper body's shielding. Conversely, the dosimeters exhibit similar doses with a ~3% deviation because they are oriented towards the AP direction. Besides, the statistical uncertainty of D_{Det} is about 7% ($k = 2$), exceeding the uncertainty of dosimeter placement. The DCCs in all cases range between 0.5 and 1, confirming the validity of

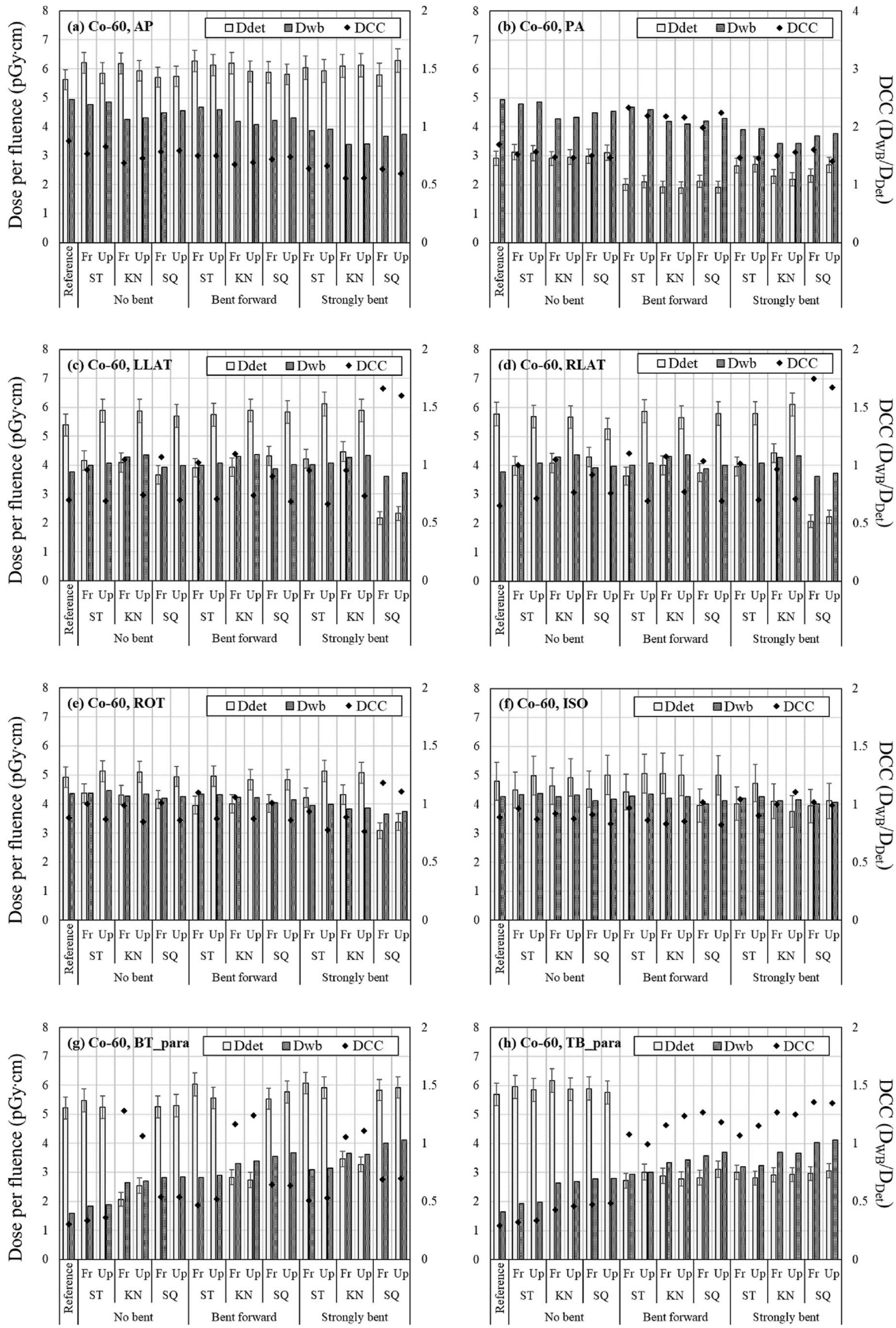

Fig. 4. Dose per fluences (Left-hand axis) of the whole-body (Dwb) and detector (Ddet) and DCCs (Right-hand axis) of the postures shown in Fig. 1 under parallel exposure of (a) AP, (b) PA, (c) LLAT, (d) RLAT, (e) ROT, (f) ISO, (g) BT_{para}, and (h) TB_{para} beams of Co-60. Abbreviations for postures: Fr is Front hands, Up is Up hands, ST is Standing, KN is Kneeling, SQ is squatting, and Reference indicates the M111 posture.

existing radiation protection approaches for AP exposure.

Fig. 4 (b) shows a similar reduction trend in the D_{WB} according to the degree of bending. However, the lowest D_{Det} values are found in the medium-bent postures (~45°). The higher D_{Det} values in the strongly bent postures (~90°) are presumed to be mainly due to the thigh shielding rather than torso shielding. As a result, for all postures, the DCCs exceed 1, reaching a maximum of 2.3 for the medium-bent postures.

Fig. 4 (c) and (d) present the results of the lateral exposures. Considering the symmetry, the behavior of the data for both exposures is similar. Excluding the two squatting postures with strongly-bent-forward, the D_{WB} of the rest shows a deviation of about 4%, with the former being roughly 10% lower than the average of the rest. Due to the arm shielding, the D_{Det} decreased by an average of 30%, with a maximum decrease of 36%. The uncertainty of dosimeter placement can be more significant in the lateral exposures, but these deviations were still within the statistical uncertainty of the calculation. For the two squatting postures with strongly-bent-forward, additional shielding from the thighs results in significantly lower D_{Det}. Therefore, a DCC of 1.7 is observed for these postures, while the rest range from 0.6 to 1.1.

In Fig. 4 (e), mitigated shielding effects were observed for all conditions as the data indicates the average of the previous four exposure directions. Additionally, highly uniform doses across the postures and dosimeters were found for the ISO setup in Fig. 4 (f).

In Fig. 4 (g) and (h), it should be mentioned that these exposure setups are unrealistic and were applied solely to evaluate the geometrical effect of the modified posture phantoms. In both exposures, the D_{WB} has a trend proportional to the degree of torso bending and the degree of body compression, i.e. in the order of standing-kneeling-squatting. D_{Det} is predominantly influenced by the thigh shielding in BT_{para} and by the torso bending in the TB_{para} exposure. The DCCs range from 0.3 to 1.4, showing the highest posture-dependent deviations across all exposure directions.

The highest DCC observed for all results occurs at the PA exposure with the medium-bent postures, while the lowest DCCs are identified in the BT_{para} and TB_{para} exposures with no torso bending. For AP, LLAT, RLAT, ROT, and ISO exposures, except for the squatting postures with strongly-bent-forward, the DCCs predominantly range between 0.5 and 1.1. Strong posture dependence was observed for the DCCs at the BT_{para} and TB_{para} setup, necessitating further investigation with more realistic radiation fields. The contribution of the scattering effect of secondary particles was negligible compared to the shielding effect. Similar results were found with Ir-192 and Cs-137 isotopes, with an increased attenuation effect at lower energies. To enhance data utilization in future studies and provide modifying factors for the reference standing posture, the ratios of each DCC to the reference phantom are presented in Table A1 of the Supplementary Material.

The data in Fig. 4 is too scattered to isolate the effects of individual postures, so it was reorganized as shown in Fig. 5. The 19 postures were grouped based on torso bending, leg shape, and hand position to analyze the trends in D_{WB} relative to the reference posture. Since averaging data for discrete-shaped postures is not feasible, the data for each group was presented as a scatter plot. The impact of torso bending was most evident in the AP, PA, ROT, BT_{para}, and TB_{para} beams, where the D_{WB} ratios decreased (up to 0.7–0.8) in the AP and PA beams and increased (up to 2.0–2.7) in the BT_{para} and TB_{para} beams as increasing the degree of bending. For the leg shape, the kneeling postures showed a decreasing trend for AP and PA beams, and an increasing trend in LLAT and RLAT beams. In the BT_{para} and TB_{para} beams, the effect of leg shape was similar to that of torso bending. The grouping based on the hand position showed a wide data distribution, but the differences between the two positions were negligible. Overall, the degree of torso bending and leg shape were the most influential factors affecting D_{WB} variation, particularly in the BT_{para} and TB_{para} beams.

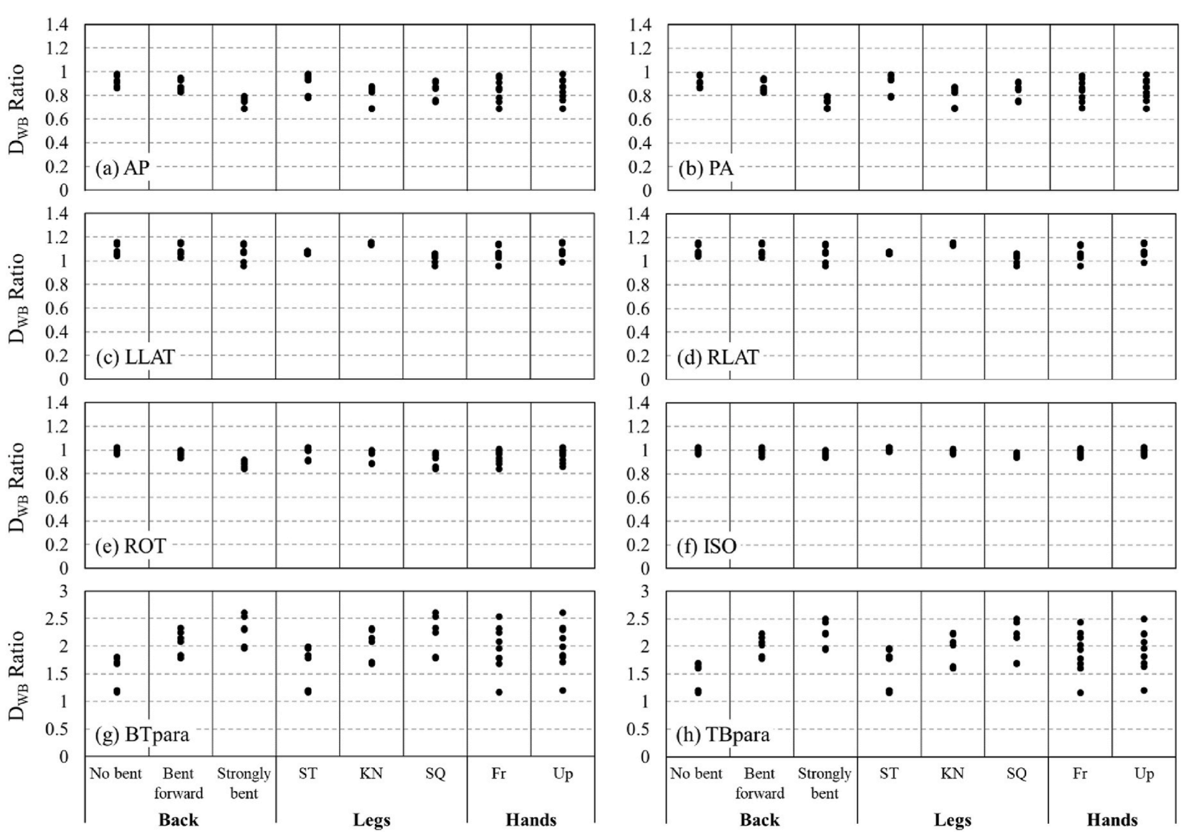

Fig. 5. D_{WB} ratios of posture-modified phantoms to the reference phantom (M111) across grouped postures under Co-60 beam exposures from (a) AP, (b) PA, (c) LLAT, (d) RLAT, (e) ROT, (f) ISO, (g) BTpara, and (h) TBpara. Posture abbreviations: Fr – Front hands, Up – Up hands, ST – Standing, KN – Kneeling, SQ – Squatting.

Although the phantom types differ, comparing the results with previous studies offers valuable insights into the impact of posture on dose evaluation. Dewji et al. (2017) assessed effective dose coefficients using PIMAL phantoms with 45° and 90° torso bending in AP, PA, LLAT, RLAT, and ISO fields, comparing these to an upright phantom. Table 1 presents a comparison of overlapping data between the previous and current studies. Since different dose units (effective dose vs. D_{WB}) and beam energies were used in each study, direct data comparison is challenging. To address this, we calculated effective dose ratios or D_{WB} ratios between the torso-bending and standing postures to evaluate the relative impact of posture variations under the same exposure geometry. Since there was no overlapping energy range between the two datasets, 1 MeV and Co-60 were compared. The dose data of the M111, M212, and M312 postures were used for standing, 45°, and 90° torso bending, respectively. For the standing posture under AP exposure, the effective dose of the PIMAL phantom was 4.51 pSv•cm^2, while the D_{WB} of the MRCP phantom was 4.93 pGy•cm^2—comparable within a 10% difference despite the different units. However, significant differences emerged in AP and PA exposures for the posture-modified phantoms. In the 45° bending posture, the PIMAL phantom showed a 20% reduction in effective dose compared to the standing posture, whereas the MRCP phantom exhibited negligible changes of around 5% in D_{WB}. In the 90° bending posture, the PIMAL phantom showed a 60–70% reduction in effective dose for AP and PA exposures, while the MRCP phantom only demonstrated about a 20% reduction for both. These differences are likely due to anatomical variations between the phantom types, such as organ location, torso thickness, and the shape of torso bending, which ultimately affect the effective dose and D_{WB} in different ways. Despite these discrepancies, the LLAT, RLAT, and ISO exposures showed differences within ±5% between the two studies. Further investigation is necessary to fully understand the impact of posture variations across different phantom types.

3.3. Standing posture in BT_{iso} and TB_{iso}

DCCs of the reference standing posture (M111) in the BT_{iso} beams of Co-60 are shown in Fig. 6 (a). The DCCs decrease significantly as the beam radius increases, but beyond 20 m, the reduction is negligible. For the beams with less than a 50 cm radius, DCCs of more than 5 were calculated due to the divergence of doses between the dosimeter and the human body, which is originated by body shielding and the height-to-fluence dependency shown in Fig. 3. However, for the beams over a 20 m radius, the aforementioned effects diminished and the DCC converged to 1. A ground contamination scenario with a narrow radius is somewhat arbitrary. Besides, wider beams showing negligible changes in DCC are not in the interest of this study. Therefore, the BT_{iso} beam radius from 1 to 20 m was considered for further investigation regarding the modified postures in the next section.

Fig. 6 (b) presents the DCCs in the TB_{iso} beams of Co-60. In the TB_{iso} beams, the dosimeter was located where the body shielding effect was

Table 1
Effective dose (D_E) ratios and D_{WB} ratios between the torso-bending (45° and 90°) and standing postures (i.e. D_E(ST) and D_{WB}(ST)) under AP, PA, LLAT, RLAT, and ISO exposures. The effective dose ratios were referenced from a previous study* using deformed PIMAL phantoms at 1 MeV energy (Dewji et al., 2017), while the D_{WB} ratios were calculated for the M111, M212, and M312 postures under Co-60 exposure.

	PIMAL* (D_E(45°)/ D_E(ST))	MRCP (D_{WB}(45°)/ D_{WB}(ST))	PIMAL* (D_E(45°)/ D_E(ST))	MRCP (D_{WB}(45°)/ D_{WB}(ST))
AP	–	0.95	0.39	0.78
PA	0.79	0.95	0.29	0.79
LLAT	1.13	1.06	1.13	1.07
RLAT	1.12	1.06	1.12	1.07
ISO	0.99	1.00	0.99	0.99

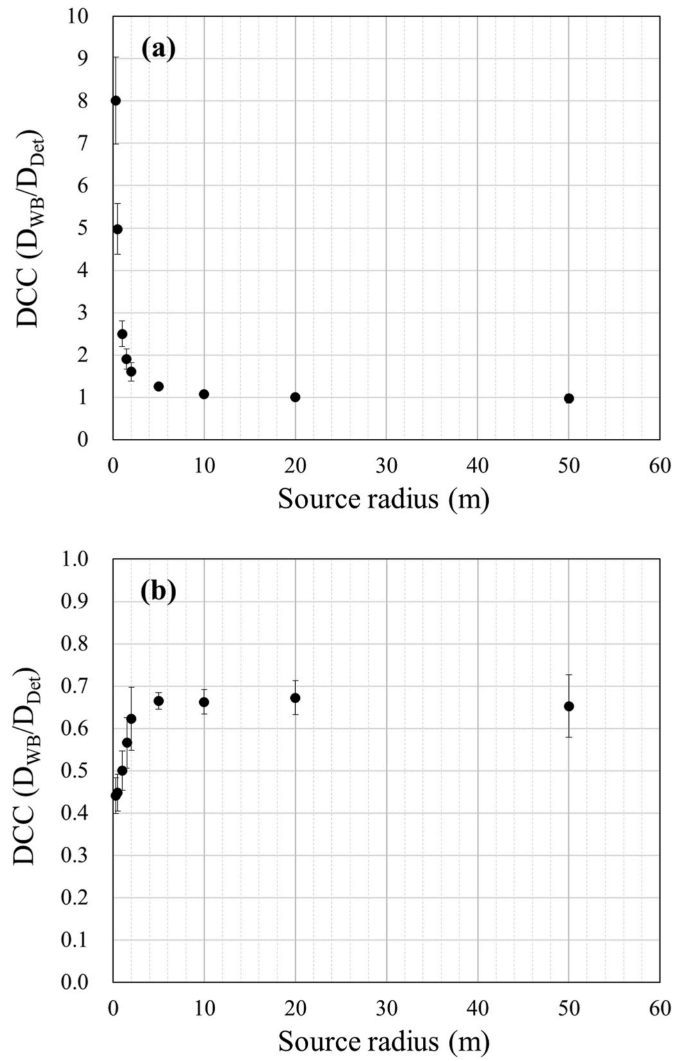

Fig. 6. DCCs of the reference standing posture (M111) in relation to the source radius in (a) BT_{iso} and (b) TB_{iso} beams of Co-60.

lower than in the BT_{iso} beams because the top of the MRCP was placed 75 cm below the ceiling. Therefore, below a 2 m radius, the reduced DCC is assumed to be predominantly due to the height-to-fluence dependency. Above a 5 m radius, relatively homogeneous DCCs were observed. In the 50 m radius beam, where the fluence is considered relatively uniform, BT_{iso} and TB_{iso} have distinct DCCs of 1 and 0.67, respectively. In both cases, the dosimeter was positioned at a similar distance of ~120 cm from the source surface, exhibiting a dose variation of less than 10%. Conversely, the D_{WB} showed a ~30% lower value in TB_{iso} compared to BT_{iso}. Given the changes in DCC and the realistic workplace for ceiling contamination, such as steam generators, further investigations considered contamination structures with a source radius of 1~10 m.

3.4. Various postures in BT_{iso} and TB_{iso}

In the BT_{iso} beams, DCCs for various postures can be influenced by multiple variables. For instance, both the dosimeter and the human body are affected by the height-to-fluence dependency and partial shielding, which complicates the analysis. Nonetheless, the leg shapes, which had a significant impact on DCCs in the BT_{para} beam, can be used to classify the data as shown in Fig. 7 (a) to (c). The postures and corresponding labels were included as insets for individual plots. Error bars were omitted for the visuality of the data. The analysis was done to find a posture

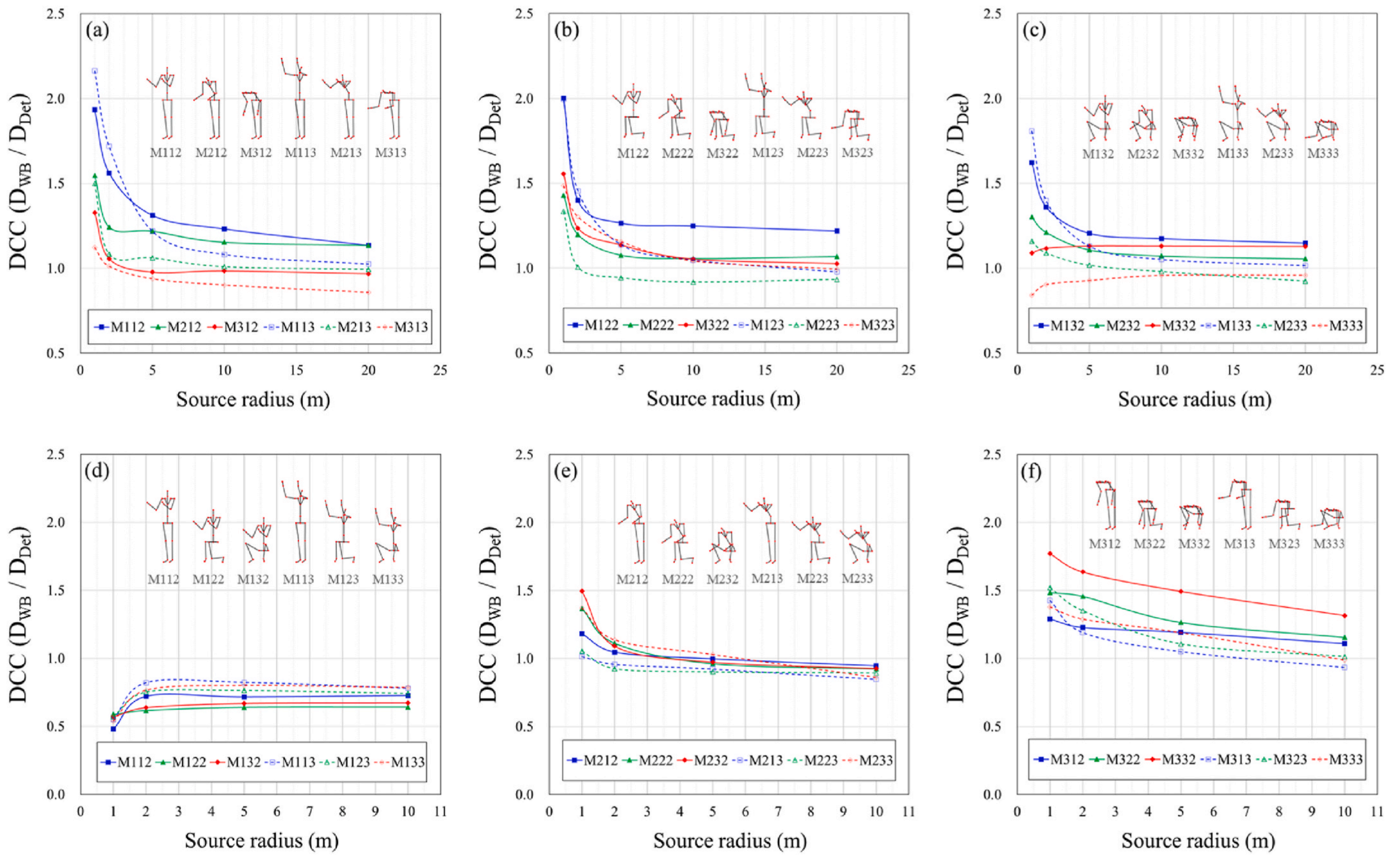

Fig. 7. DCCs of various postures in relation to the source radius in (a–c) BT_{iso} and (d–f) TB_{iso} beams of Co-60.

dependency and to estimate a range of DCCs in a given scenario, rather than provide a detailed analysis of the DCCs.

Most DCCs decrease as the radius increases, tending to converge towards 1 over a 10 m radius. In contrast, M332 and M333 show opposite behavior, increasing DCC with the radius, which is due to the significant shielding effect of the dosimeter against the lateral beam in these more crouched postures. Contrary to the expectation, the shape of the lower body was not a major factor influencing DCCs. Postures with different leg shapes, such as M112, M122, and M132, or M113, M123, and M133, exhibited a similar decreasing trend of DCCs. Instead, in most cases, D_{Det} increased as the height from the floor decreased in the order of standing, kneeling, and squatting. Similarly, the effect of torso bending results in lowering the DCC by increasing D_{Det} as the dosimeter faces and is brought closer to the floor. For example, comparing M112, M212, and M312, the difference in D_{WB} increased by up to 15%, while D_{Det} increased by up to 70%. The M323, M332, and M333 postures had higher DCC values than expected due to the strong shielding of the legs and arms adjacent to the dosimeter. The effect of hand locations was predominantly influential over a 5 m radius. Comparing postures with different hand positions, such as M112 & M113, M122 & M123, and M322 & M323, shows a DCC difference of 3–20% at 20 m. As a result, DCC in the BT_{iso} beams was primarily influenced by the degree of torso bending. Comparing M113 and M313, the DCC difference was about 50% at a 1 m radius. As the beam radius increased and fluence became more uniform, the difference reduced to 16% at a 20 m radius. Additionally, across all postures, DCC values ranged from 0.84 to 2.5 at 1 m, 0.9 to 1.72 at 2 m, and 0.86 to 1.22 at 20 m. This implies a potential underestimation of Hp(10) in narrow-radius contamination scenarios.

In the TB_{iso} beams, the data were displayed based on the torso shielding, as shown in Fig. 7 (d)–(f): no-bent, bent-forward, and strongly-bent-forward. Depending on the radius, DCC showed an increasing trend in no-bent postures and a decreasing trend in bent-forward (~45°) and strongly-bent-forward (~90°) postures. Additionally, beyond a 2 m radius, no-bent and bent-forward postures exhibited relatively consistent DCC values. At a 2 m radius, the approximate width of an arbitrary steam generator (Kim and Kong, 2010), DCC ranged from 0.6 to 0.8 in no-bent postures, from 0.9 to 1.2 in bent-forward (~45°) postures, and from 1.2 to 1.7 in strongly-bent-forward (~90°) postures. Notably, in working postures involving the most crouched one, such as M332 in strongly-bent-forward, DCC reached up to 1.8, underscoring the need for dose conversion. The influence of leg shape on DCC is attributed to the height-to-fluence dependency, showing about a 10% difference at a 2 m beam when comparing M112 and M132. The impact of hand position is primarily observed in no-bent postures and is largely due to lateral shielding. When comparing M132 and M133, there was approximately a 20% difference beyond a 2 m radius.

The same data sets for Cs-137 and Ir-192 isotopes are presented in Figs. A3 and A4, respectively, and the ratios of each data point to the reference phantom are provided in Table A2 of Supplementary Material.

4. Conclusions

The present study investigated the necessity of dose conversion considering working postures, especially in radiological accident scenarios. By using the adult male MRCP and Geant4 simulation code, the DCCs of 19 representative working postures under several exposure geometries were calculated. While current radiation protection systems that assume a standing posture are valid in most situations, it has been recognized that there can be significant differences between a personal dosimeter and the dose received by workers with various postures under specific exposure geometries. Specifically, the degree of torso bending and the positions of the arms and legs significantly influenced the DCCs due to body shielding effects. In semi-isotropic beams, such as scenarios with floor and ceiling contamination, the fluence according to the beam area and distance also played a role. In the BT_{iso} beams, the degree of torso bending had a considerable effect, with DCC values ranging from 0.8 to 2.5 at a 1 m beam radius and converging to 0.9 to 1.25 at a 20 m beam radius. This emphasizes the need for posture-specific dose assessment in narrow-radius contamination scenarios. In the TB_{iso} beams, for beam radius greater than 2 m, the DCCs were less than 1.2 with no-bent or bent-forward cases, while in the strongly-bent-forward case, the DCC significantly increased as the beam radius decreased. This implies that the dose conversion approach will be effective in compensating for strong shielding effects in work environments, such as a steam generator, that requires crouching postures.

It should be emphasized that the current study preliminarily evaluated the dosimetric impact of arbitrary working postures under limited exposure geometries. Therefore, rather than being used as indicators for dose conversion in dynamic working environments, the results of this study should be read to estimate the dose range that includes postural effects, especially in unexpected radiological accidents. Further studies are needed to examine the impact of diverse non-homogeneous exposure geometries and their interaction with dynamic working postures. Additionally, future research could explore how different postures affect organ doses, considering the anatomical structure of various types of computational phantoms.

CRediT authorship contribution statement

Min Chae Kim: Writing – review & editing, Writing – original draft, Visualization, Validation, Resources, Methodology, Investigation, Formal analysis, Data curation, Conceptualization. **Hyoungtaek Kim:** Writing – review & editing, Writing – original draft, Validation, Supervision, Resources, Methodology, Investigation, Formal analysis, Data curation, Conceptualization. **Heagin Han:** Writing – review & editing, Software. **Yoomi Choi:** Data curation, Conceptualization. **Sora Kim:** Writing – review & editing, Resources, Project administration, Conceptualization. **Jungil Lee:** Conceptualization. **Byung Il Min:** Resources. **Kyungsuk Suh:** Resources. **Chan Hyeong Kim:** Writing – review & editing, Software, Resources, Conceptualization.

Declaration of competing interest

The authors declare the following financial interests/personal relationships which may be considered as potential competing interests: Hyoungtaek Kim reports financial support was provided by Korea Ministry of Science and ICT. If there are other authors, they declare that they have no known competing financial interests or personal relationships that could have appeared to influence the work reported in this paper.

Acknowledgments

The study was carried out under the National Research Foundation of Korea (NRF) grant funded by the Korea government (Ministry of Science and ICT) (RS-2022-00144350).

Appendix A. Supplementary data

Supplementary data to this article can be found online at https://doi.org/10.1016/j.radphyschem.2024.112413.

Data availability

Data will be made available on request.

References

Akkurt, H., Eckerman, K.F., 2007. Development of PIMAL: Mathematical Phantom with Moving Arms and Legs. Oak Ridge National Lab.(ORNL), Oak Ridge, TN (United States).

Bales, K., Dewji, S., 2019. Comparison of organ and effective photon dose coefficients for reference phantoms in articulated and upright postures in cranial and caudal irradiation geometries. Health Phys. 116, 599–606.

Breazeal, N.L., Davis, K.R., Watson, R.A., Vickers, D.S., Ford, M.S., 1996. Simulation-based Computation of Dose to Humans in Radiological Environments. Sandia National Labs.

Clairand, I., Huet, C., Trompier, F., Bottollier-Depois, J.-F., 2008. Physical dosimetric reconstruction of a radiological accident due to gammagraphy equipment that occurred in Dakar and Abidjan in summer 2006. Radiat. Meas. 43, 698–703.

Dewji, S., Reed, K.L., Hiller, M., 2017. Comparison of photon organ and effective dose coefficients for PIMAL stylized phantom in bent positions in standard irradiation geometries. Radiat. Environ. Biophys. 56, 277–291.

Dockrell, S., O'Grady, E., Bennett, K., Mullarkey, C., Mc Connell, R., Ruddy, R., Twomey, S., Flannery, C., 2012. An investigation of the reliability of Rapid Upper Limb Assessment (RULA) as a method of assessment of children's computing posture. Appl. Ergon. 43, 632–636.

Eakins, J., Kouroukla, E., 2015. Luminescence-based retrospective dosimetry using Al2O3 from mobile phones: a simulation approach to determine the effects of position. J. Radiol. Prot. 35, 343.

Eakins, J.S., Ainsbury, E.A., 2018. Quantities for assessing high photon doses to the body: a calculational approach. J. Radiol. Prot. 38, 743.

Endo, A., Yamaguchi, Y., 2003. Analysis of dose distribution for heavily exposed workers in the first criticality accident in Japan. Radiat. Res. 159, 535–542.

Han, H., Kim, J., Moon, S., Son, G., Shin, B., Kim, H., Kim, S., Choi, C., Kim, C.H., 2023. MPPD: a user-friendly posture deformation program for mesh-type computational phantoms. Health Phys. 10, 1097.

Hayashi, K., Hirayama, H., Iwanaga, K., Kondo, K., Suzuki, S., 2024. Estimation of 137Cs contamination density of wall, ceiling, and floor at unit 2 operation floor in fukushima daiichi nuclear power station using pinhole gamma camera. Nucl. Sci. Eng. 198, 207–227.

Hirouchi, J., Takahara, S., Yoshimura, K., 2021. Indoor and outdoor radionuclide distribution in houses after the fukushima dai-ichi nuclear power plant accident. J. Environ. Radioact. 232, 106572.

ICRP, 2007. ICRP Publication 103. The 2007 Recommendations of the International Commission on Radiological Protection.

ICRP, 2010. ICRP Publication 116, Conversion Coefficients for Radiological Protection Quantities for External Radiation Exposures.

ICRP, 2020a. ICRP Publication 144, Dose Coefficients for External Exposures to Environmental Sources.

ICRP, 2020b. ICRP Publication 145 : adult mesh-type reference computational phantoms. SAGE journals.

Imanaka, T., Hayashi, G., Endo, S., 2015. Comparison of the accident process, radioactivity release and ground contamination between Chernobyl and Fukushima-1. J. Radiat. Res. 56, i56–i61.

Karhu, O., Kansi, P., Kuorinka, I., 1977. Correcting working postures in industry: a practical method for analysis. Appl. Ergon. 8, 199–201.

Kim, H.G., Kong, T.Y., 2010. Selection of the most appropriate two-dosemeter algorithm for estimating effective dose equivalent during maintenance periods in Korean nuclear power plants. Radiat. Protect. Dosim. 140, 171–181.

Kim, M.C., Kim, H., Han, H., Lee, J., Lee, S.K., Chang, I., Kim, J.-L., Kim, C.H., 2019. A study on dose conversion from a material to human body using mesh phantom for retrospective dosimetry. Radiat. Meas. 126.

Schaub, K.G., Mühlstedt, J., Illmann, B., Bauer, S., Fritzsche, L., Wagner, T., Bullinger-Hoffmann, A.C., Bruder, R., 2012. Ergonomic assessment of automotive assembly tasks with digital human modelling and the 'ergonomics assessment worksheet'(EAWS). Int. J. Hum. Factors Model Simulat. 3, 398–426.

Vazquez, J.A., Ding, A., Haley, T., Caracappa, P.F., Xu, X.G., 2014. A dose-reconstruction study of the 1997 Sarov criticality accident using animated dosimetry techniques. Health Phys. 106, 571–582.

Veinot, K.G., Eckerman, K.F., Hertel, N.E., 2016. Organ and effective dose coefficients for cranial and caudal irradiation geometries: photons. Radiat. Protect. Dosim. 168, 167–174.

Werner, C.J., Bull, J., Solomon, C., Brown, F., McKinney, G., Rising, M., Dixon, D., Martz, R., Hughes, H., Cox, L., 2018. MCNP6. 2 Release Notes. Los Alamos National Laboratory report LA-UR-18-20808.

Yeom, Y.S., Han, H., Choi, C., Nguyen, T.T., Shin, B., Lee, C., Kim, C.H., 2019. Posture-dependent dose coefficients of mesh-type ICRP reference computational phantoms for photon external exposures. Phys. Med. Biol. 64, 075018.